

# A three-dimensional wavelet based multifractal method : about the need of revisiting the multifractal description of turbulence dissipation data

Pierre Kestener and Alain Arneodo

Laboratoire de Physique, Ecole Normale Supérieure de Lyon, 46 allée d'Italie, 69364 Lyon cédex 07, France

(Dated: May 22, 2019)

We generalize the wavelet transform modulus maxima (WTMM) method to multifractal analysis of 3D random fields. This method is calibrated on synthetic 3D monofractal fractional Brownian fields and on 3D multifractal singular cascade measures as well as their random function counterpart obtained by fractional integration. Then we apply the 3D WTMM method to the dissipation field issue from 3D isotropic turbulence simulations. We comment on the need to revisiting previous box-counting analysis which have failed to estimate correctly the corresponding multifractal spectra because of their intrinsic inability to master non-conservative singular cascade measures.

PACS numbers: 47.53.+n, 02.50.Fz, 05.40-a, 47.27.Gs

The multifractal formalism was introduced in the mid-eighties to provide a statistical description of the fluctuations of regularity of singular measures found in chaotic dynamical systems [1] or in modelling the energy cascading process in turbulent flows [2, 3, 4]. Box-counting algorithms were successfully adapted to resolve multifractal scaling for isotropic self-similar fractals [3, 5]. As to self-affine fractals, Parisi and Frisch [6] developed, in the context of turbulence velocity data analysis, an alternative multifractal description based on the investigation of the scaling behavior of the moments of the velocity increments, the so-called structure functions. Unfortunately, there are some drawbacks to these classical multifractal methods and as proposed in Ref. [7], a natural way of performing a unified multifractal analysis of both singular measures and multi-affine functions, consists in using the *continuous wavelet transform* (WT). By using wavelets instead of boxes, one can take advantage of the freedom in the choice of these “generalized oscillating boxes” to get rid of possible smooth behavior that might either mask singularities or perturb the estimation of their strength. Applications of the so-called WTMM method to 1D signals have already provided insight into a wide variety of problems, *e.g.* fully-developed turbulence, financial markets, meteorology, physiology, DNA sequences [8, 9]. In a recent work [10], the WTMM method has been generalized to 2D with the specific goal to achieve multifractal analysis of rough surfaces. The new 2D algorithms have been successfully applied to characterize the intermittent nature of satellite images of the cloud structure [11] and to assist in the diagnosis in digitized mammograms [12]. Our aim here is to go one step further and to generalize the WTMM method from 2D to 3D, starting from the original theoretical concepts and following the same methodological steps.

The 3D WTMM method consists in smoothing the discrete 3D field data by convolving it with a filter and then in computing the gradient on the smoothed signal in a manner inspired from multiscale edge detectors [13]. Define three wavelets  $\psi_i(x, y, z) = \partial\phi(x, y, z)/\partial x_i$  with  $x_i =$

$x, y$  or  $z$  for  $i = 1, 2$  or  $3$  respectively and  $\phi(x, y, z)$  is a 3D smoothing function well localized around  $x = y = z = 0$ . For any function  $f(x, y, z) \in L^2(\mathbb{R}^3)$ , the WT with respect to  $\psi_1, \psi_2$  and  $\psi_3$  at the point  $\mathbf{b}$  and scale  $a$  has three components, and thus can be expressed in a vectorial form [10, 13] :

$$\mathbf{T}_\psi[f](\mathbf{b}, a) = \nabla\{\phi_{\mathbf{b},a} * f\}, \quad (1)$$

where  $\phi_{\mathbf{b},a}(\mathbf{r}) = a^{-3}\phi(a^{-1}(\mathbf{r}-\mathbf{b}))$ . If  $\phi$  is just a Gaussian  $\phi(\mathbf{r}) = \exp(-\mathbf{r}^2/2)$  (or one of its derivatives), then Eq. (1) defines the 3D WT as the gradient field vector of  $f(\mathbf{r})$  smoothed by dilated versions  $\phi(\mathbf{r}/a)$  of this filter. At a given scale  $a$ , the WTMM are defined by the positions  $\mathbf{b}$  where the WT modulus  $\mathcal{M}_\psi[f](\mathbf{b}, a) = |\mathbf{T}_\psi[f](\mathbf{b}, a)|$  is locally maximum along the direction of the WT vector (Eq. (1)). These WTMM lie on connected surfaces hereafter called *maxima surfaces* (see Fig. 2). In theory, at each scale  $a$ , one only needs to record the position of the local maxima of  $\mathcal{M}_\psi$  (WTMMM) along the maxima surfaces together with the value of  $\mathcal{M}_\psi[f]$  and the WT vector direction. They indicate locally the direction where the signal has the sharpest variation. These WTMMM are disposed along connected curves across scales called *maxima lines* [10, 13] living in a 4D space  $(x, y, z, a)$ . We will define the WT skeleton as the set of maxima lines that converge to the  $(x, y, z)$ -hyperplane in the limit  $a \rightarrow 0^+$  (Fig 2(d)). One can prove [10, 13] that, provided the first  $n_\psi$  moments of  $\psi$  be zero, then  $\mathcal{M}_\psi[f](\mathcal{L}_{\mathbf{r}_0}(a)) \sim a^{h(\mathbf{r}_0)}$  along the maxima line  $\mathcal{L}_{\mathbf{r}_0}(a)$  pointing to the point  $\mathbf{r}_0$  in the limit  $a \rightarrow 0^+$ , where  $h(\mathbf{r}_0) (< n_\psi)$  is the local Hölder exponent of  $f$ . As in 1D and 2D [7, 10], the 3D WTMM method consists in defining the following partition functions :

$$\mathcal{Z}(q, a) = \sum_{\mathcal{L} \in \mathcal{L}(a)} (\mathcal{M}_\psi[f](\mathbf{r}, a))^q \sim a^{\tau(q)}, \quad (2)$$

where  $q \in \mathbb{R}$  and  $\mathcal{L}(a)$  is the set of maxima lines of the WT skeleton. Then from Legendre transforming  $\tau(q): D(h) = \min_q(qh - \tau(q))$ , one gets the  $D(h)$  singularity

spectrum defined as the Hausdorff dimension of the set of points  $\mathbf{r}$  where  $h(\mathbf{r})$  is  $h$ . As an alternative strategy one can compute the mean quantities  $h(q, a)$  and  $D(q, a)$  :

$$h(q, a) = \sum_{\mathcal{L} \in \mathcal{L}(a)} \ln |\mathcal{M}_\psi[f](\mathbf{r}, a)| W_\psi[f](q, \mathcal{L}, a), \quad (3)$$

$$D(q, a) = \sum_{\mathcal{L} \in \mathcal{L}(a)} W_\psi[f](q, \mathcal{L}, a) \ln(W_\psi[f](q, \mathcal{L}, a)), \quad (4)$$

where  $W_\psi[f](q, \mathcal{L}, a) = (\mathcal{M}_\psi[f](\mathbf{r}, a))^q / \mathcal{Z}(q, a)$  is a Boltzmann weight computed from the WT skeleton. From the scaling behavior of these quantities, one can extract  $h(q) = \lim_{a \rightarrow 0^+} h(q, a) / \ln a$  and  $D(q) = \lim_{a \rightarrow 0^+} D(q, a) / \ln a$  and therefore the  $D(h)$  spectrum.

Fractional Brownian motions (fBm) are homogenous random self-affine functions that have been specifically used to calibrate both the 1D and the 2D WTMM methodologies [7, 10]. 3D fBm  $B_H(\mathbf{r})$  are Gaussian stochastic processes with stationary increments and well-known statistical properties :  $\tau(q) = qH - 3$ ,  $0 < H < 1$ . In Fig. 1 are reported the results of the 3D WTMM method when applied to  $16 \times (256)^3$  realizations of  $B_{H=1/2}(\mathbf{r})$ . As shown in Fig. 1(a), the annealed average partition functions  $\mathcal{Z}(q, a)$  display nice scaling behavior over 3 octaves when plotted *vs*  $a$  in a logarithmic representation. When proceeding to a linear regression fit of the data, one gets, for  $q \in ]-2, 4[$ , the linear  $\tau(q)$  spectrum shown in Figure 2(c) in good agreement with the theoretical  $\tau(q)$  spectrum. This signature of monofractality is confirmed in Fig. 1(b) where, when plotting  $h(q, a)$  vs  $\log_2(a)$  (Eq. (3)),  $H = 1/2$  is shown to provide an excellent fit of the slope of the data ( $\sigma_W \lesssim a \lesssim 4\sigma_W$ ) and this independently of  $q \in ]-2, 4[$ . As shown in Fig. 1(d), when using  $h(q, a)$  (Eq. (3)) and  $D(q, a)$  (Eq. (4)) to estimate  $h(q)$  and  $D(q)$ , one gets a  $D(h)$  spectrum which, up to the numerical uncertainty, reduces to a single point  $D(h = H = 1/2) = 3$  (and  $-\infty$  for  $h \neq H$ ). Similar quantitative estimates of the  $\tau(q)$  and  $D(h)$  spectra have been obtained for 3D fBm's  $B_H(\mathbf{r})$  for  $H = 1/3$  and  $2/3$ , thus confirming that 3D fBm's are nowhere differentiable with a unique Hölder exponent  $h = H$ .

Generating multifractal measures using multiplicative cascades is a well documented subject [2, 3, 4]. The ‘‘binomial (or p-) model’’, originally designed to account for the statistical scaling properties of the dissipation field in fully developed turbulence, has very simple multifractal properties [2, 3, 4]. The 3D version of the p-model consists in starting with a cube of characteristic size  $L$ , in which a measure  $\mu = \mu_L$  is uniformly distributed. At the first step, the initial cube is broken into eight smaller cubes of size  $L/2$  and one selects at random the four sub-cubes which will receive a fraction  $M^{(1)} = p_1/4$ , the four others receiving the fraction  $M^{(2)} = p_2/4$  of the measure ( $p_1 + p_2 = 1$ ). By repeating the same procedure recursively and independently at smaller scales, one generates a random singular measure  $\mu_n(\mathbf{r}; l) =$

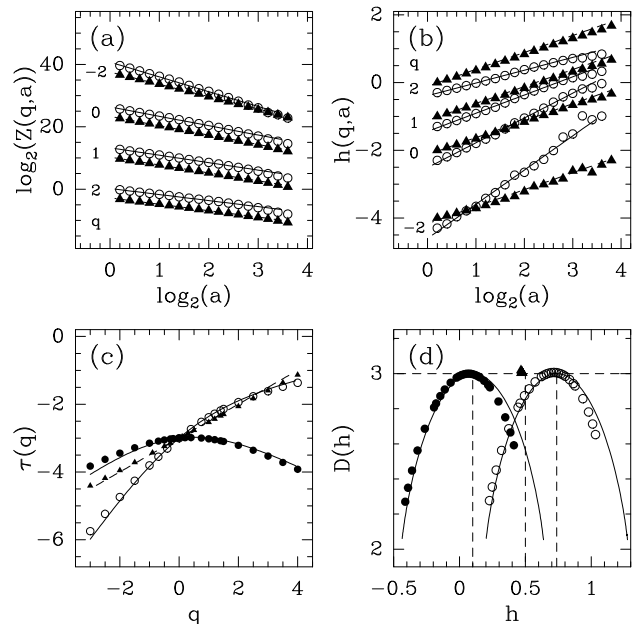


FIG. 1: Multifractal analysis of 3D  $B_{H=1/2}$  ( $\Delta$ ), 3D p-model ( $\circ$ ,  $p = 0.32$ ) and 3D FISC ( $\bullet$ ,  $p = 0.32$ ,  $H^* = 0.638$ ) data using the 3D WTMM method with a first ( $\Delta$ ) or third ( $\circ, \bullet$ ) order analyzing wavelet ( $\phi(\mathbf{r})$  is a Gaussian or its Laplacian). (a)  $\log_2 \mathcal{Z}(q, a)$  vs  $\log_2 a$ ; (b)  $h(q, a)$  vs  $\log_2 a$ ; the dashed and solid lines correspond to linear regression fits over the three first octaves. (c)  $\tau(q)$  vs  $q$ ; the dashed and solid lines correspond to the theoretical predictions. (d)  $D(h)$  vs  $h$  as obtained from the scaling behavior of  $h(q, a)$  and  $D(q, a)$ . These results correspond to annealed averaging over  $16 \times (256)^3$  images.  $a$  is expressed in  $\sigma_W$  units where  $\sigma_W = 7$  (pixels) is the characteristic size of  $\psi$  at the smallest resolved scale.

$\mu_L \prod_{i=1}^n M_i$ ,  $l/L = 2^{-n} \rightarrow 0$ . A straightforward computation yields :  $\tau_\mu(q) = -(q+2) - \log_2(p_1^q + p_2^q)$ . As a mean of introducing continuity, Fractionally Integrated Singular Cascade (FISC) algorithm [14] amounts to a low-pass power-law filtering in Fourier space:  $f_n(\mathbf{r}) = \mu_n(\mathbf{r}) * |\mathbf{r}|^{-(1-H^*)}$ ,  $0 < H^* < 1$ . This leads to FISC random functions with the following multifractal spectrum :  $\tau_f(q) = \tau_\mu(q) + qH^* = -2 - q(1-H^*) - \log_2(p_1^q + p_2^q)$ . In Fig. 1 are reported the results of the 3D WTMM analysis of the FISC model with  $p_1 = 0.32$  and  $H^* = 0.638$ . As shown in Fig. 1(a), the partition functions  $\mathcal{Z}(q, a)$  display good scaling for  $q \in ]-2, 4[$  for which statistical convergence turns out to be achieved. The corresponding  $\tau_f(q)$  spectrum is displayed in Fig. 1(c) along with the theoretical spectrum. The agreement is quite satisfactory;  $\tau_f(q)$  is nonlinear, the hallmark of multifractal scaling. This is confirmed in Fig. 1(b) where the slope of  $h(q, a)$  vs  $\log_2(a)$  clearly depends on  $q$ . From the estimate of the scaling exponents  $h(q)$  and  $D(q)$ , one gets the single-humped  $D_f(h)$  spectrum shown in Fig. 1(d). Note that some departure from the theoretical spectrum can be observed on the right-hand side of the  $D(h)$ -curve ( $q \lesssim -2$ ) indicating that the estimate of the weakest sin-

gularities would require a larger statistical sample. In Figs. 1(c) and 1(d) are also reported the results of the 3D WTMM method for the p-model data set. Again the numerical results for  $\tau_\mu(q)$  and  $D_\mu(h)$  are found in remarkable agreement with the theoretical spectra. Let us point out that the  $D_f(h)$  curve is found identical to the  $D_\mu(h)$  curve up to a translation to the right by  $H^*$ ; this is the consequence of the fractional integration which implies  $D_f(h) = D_\mu(h - H^*)$ . Altogether these results bring the numerical demonstration that our 3D WTMM methodology paves the way from multifractal analysis of singular measures to continuous multi-affine functions.

Since Kolmogorov's founding work in 1941 (K41)[4], fully developed turbulence has been intensively studied theoretically, numerically and experimentally [3, 4]. A central quantity in the K41 theory is the mean energy dissipation  $\epsilon = \frac{\nu}{2} \sum_{i,j} (\partial_j v_i + \partial_i v_j)^2$  which is supposed to be constant. Indeed,  $\epsilon$  is not spatially homogenous but undergoes local intermittent fluctuations [3, 4]. There have been early experimental attempts to measure the multifractal spectra of  $\epsilon$  [3]. Surprisingly, the simplest version of the weighted curdling models proposed by Mandelbrot [2], namely the binomial model, turns out to account reasonably well for the observed  $\tau_\epsilon(q)$  and  $f_\epsilon(\alpha)$  spectra [3]. Experimentally, single probe measurement of the longitudinal velocity requires the use of the 1D surrogate dissipation approximation  $\epsilon' = 15\nu(\partial u/\partial x)^2$  that may introduce severe bias in the multifractal analysis. 3D multifractal processing of dissipation data is at the moment feasible only for numerically simulated flows which are still somehow limited in Reynolds number to regimes where scaling just begins to manifest itself [15]. Several numerical studies<sup>15a,c</sup> agree that  $\epsilon'$  is in general more intermittent than  $\epsilon$  which is found nearly log-normal in the inertial range<sup>15b,c</sup>.

So far mainly box-counting (BC) techniques have been used to perform multifractal analysis of numerical and experimental dissipation data [3, 15]. Here we apply the 3D WTMM method to isotropic turbulence DNS data obtained by Meneguzzi with the same numerical code as in Ref. [16] but at a  $(512)^3$  resolution and a viscosity of  $5 \cdot 10^{-4}$  corresponding to a Taylor Reynolds number  $R_\lambda = 216$ . We will examine only one snapshot of the dissipation 3D spatial field. The main steps of our 3D WT computation are illustrated in Fig. 2. Focusing on a  $(64)^3$  sub-cube, we show the original  $\epsilon$  data (Fig. 2(a)), the WTMM surfaces along with the WTMM points computed at two different scales (Figs. 2(b) and 2(c)) and some projection of the WT skeleton (Fig. 2(d)). The corresponding multifractal spectra reported in Fig. 3 result from an annealed averaging over the  $8 \times (256)^3$  sub-cubes. In Fig. 3 are also shown for comparison the estimates obtained with BC techniques. Let us point out that the WTMM definition of the  $\tau_\epsilon^{WT}(q)$  spectrum (Eq. (2)) slightly differs from the BC definition  $\tau_\epsilon^{BC}(q)$  found in the literature [3]

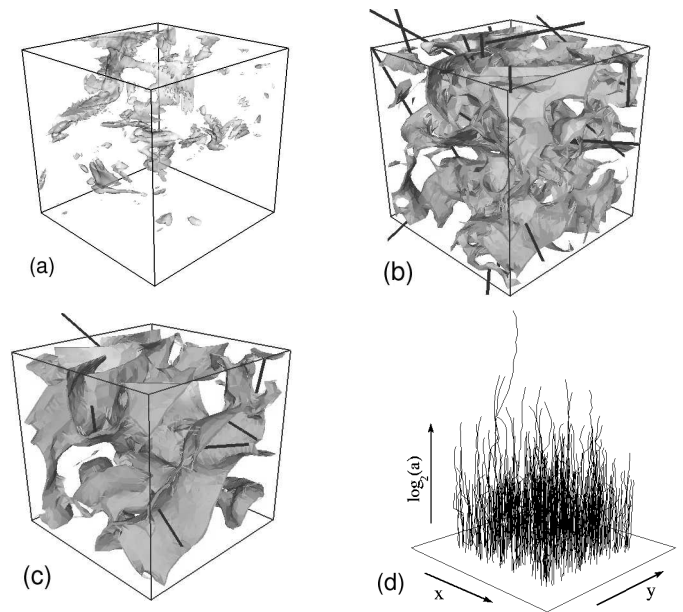


FIG. 2: 3D WT analysis of the DNS dissipation field  $\epsilon$ .  $\psi$  is the first-order analyzing wavelet ( $\phi(\mathbf{r})$  is the Gaussian). (a) Isosurface plot of  $\epsilon$  in a  $(64)^3$  sub-cube. (b) WTMM surfaces at scale  $a = 2\sigma_W$ ; from the local maxima (WTMMM) of  $\mathcal{M}_\psi$  along these surfaces originate a black segment whose length is proportional to  $\mathcal{M}_\psi$  and direction is along the WT vector. (c) same as in (b) for  $a = 4\sigma_W$ . (d) 3D projection of the WT skeleton obtained by linking the WTMMM across scales.

:  $\tau_\epsilon^{BC}(q) = \tau_\epsilon^{WT}(q) + dq = (q-1)D_q$ , which implies the following relationship  $f_\epsilon^{BC}(\alpha) = D_\epsilon^{WT}(h = \alpha - d)$  between the corresponding singularity spectra ( $d = 3$ ). By plotting  $\mathcal{Z}(q, a)/(\mathcal{Z}(q = 0, a))^q$  vs  $a$  in a logarithmic representation in Fig. 3(a), one can then directly compare  $(\mathcal{Z}(q = 0, a) \sim a^{-d})$  our WTMM computations with BC ones. Actually, for  $q \in ]-2, 4[$ , rather good scaling properties are observed. When proceeding to linear regression fits of the data, one gets the non-linear  $\tau_\epsilon(q)$  spectra shown in Fig. 3(c) that significantly deviate from a straight line, the hallmark of multifractality. But surprisingly,  $\tau_\epsilon^{WT}(q)$  significantly differs from  $\tau_\epsilon^{BC}(q) - 3q$ . Actually, most of the difference comes from the fact that our 3D WTMM algorithms reveals that the cancellation exponent [17] is definitely different from zero :  $\tau_\epsilon^{WT}(q = 1) + 3 = -0.19 \pm 0.03 < 0$ , the signature of a signed measure. Indeed, as shown in Fig. 3(c),  $\tau_\epsilon^{WT}(q)$  data are rather nicely fitted by the theoretical spectrum  $\tau_\mu(q)$  of the non-conservative p-model with  $p_1 = 0.36$  and  $p_2 = 0.78$ , which leads to  $p_1 + p_2 = 1.14 > 1$ . Unfortunately, BC methods fail to master non-conservative singular cascades since, by construction, the fact that the measure in a given box is the sum of the measures in smaller non-overlapping boxes, implies that the cancellation exponent  $\tau_\epsilon^{WT}(q = 1) = 0$ . This means that BC algorithms systematically provide a misleading conservative  $\tau_\epsilon(q)$  spectrum diagnostic with  $p = p_1/(p_1 + p_2)$  and

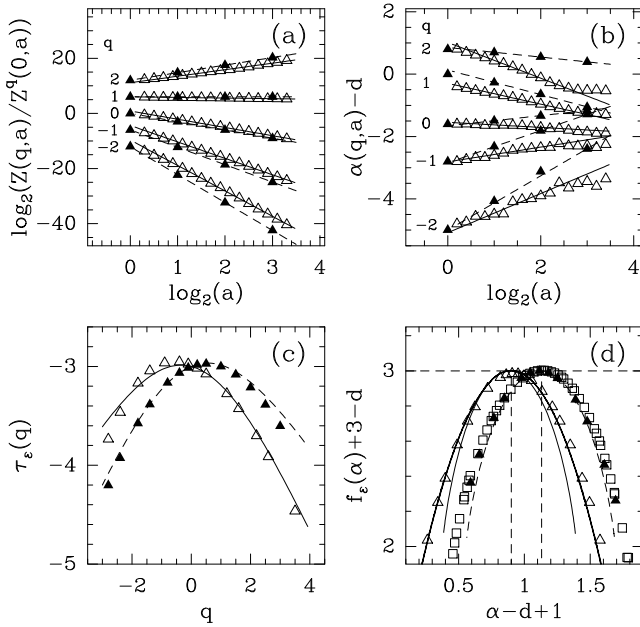


FIG. 3: Multifractal analysis of DNS dissipation data ( $d = 3$ ) using the 3D WTMM method ( $\Delta$ ) and BC techniques ( $\blacktriangle$ ). (a)  $\log_2 \mathcal{Z}(q, a) / (\mathcal{Z}(q = 0, a))^q$  vs  $\log_2 a$ ; (b)  $h(q, a) = \alpha(q, a) - 3$  vs  $\log_2 a$ ; the solid and dashed lines correspond to linear regression fits over  $\sigma_W \lesssim a \lesssim 2^3 \sigma_W$ . (c)  $\tau_\epsilon(q) = \tau_\epsilon^{WT}(q)$  or  $\tau_\epsilon^{BC}(q) - 3q$  vs  $q$ ; the solid (dashed) lines correspond to the p-model prediction with  $p_1 = 0.36$ ,  $p_2 = 0.78$  ( $p_1 = 0.32$ ,  $p_2 = 0.68$ ). (d)  $f_\epsilon(\alpha) + 3 - d$  vs  $\alpha - d + 1$ , where  $f_\epsilon(\alpha) = f_\epsilon^{BC}(\alpha)$  or  $f_\epsilon^{WT}(\alpha) = D_\epsilon^{WT}(h = \alpha - d)$ ; the solid and dashed lines have the same meaning as in (c); the thick solid line is the parabolic log-normal spectrum  $f_\epsilon(\alpha) = d - (\alpha - d + 1 - C_1)^2 / 2C_2$  with  $C_1 = 0.91$  and  $C_2 = 0.22$ . The symbols ( $\blacksquare$ ) correspond to some average  $f(\alpha)$  spectrum of experimental ( $d = 1$ ) surrogate dissipation data [3].

$1 - p = p_2 / (p_1 + p_2)$ . As shown in Fig. 3(c),  $\tau_\epsilon^{BC}(q) - 3q$  data are quite well reproduced by the theoretical conservative p-model spectrum with  $p = 0.32 = p_1 / (p_1 + p_2) = 0.36 / 1.14$ , consistently with our 3D WTMM finding for  $\tau_\epsilon^{WT}(q)$ . A straightforward calculation shows that  $\tau_\epsilon^{BC}(q) = (\tau_\epsilon^{WT}(q) + 3q) + q \log_2(p_1 + p_2)$ , i.e. the difference between the two spectra is nothing but a fractional integration of exponent  $H^* = \log_2(p_1 + p_2) \sim 0.19$ . This result is confirmed in Fig. 3(d) where the singularity spectrum  $f_\epsilon^{BC}(\alpha)$  is misleadingly shifted to the right by  $H^* \sim 0.19$  without any shape change as compared to the  $f_\epsilon^{WT}(\alpha) = D_\epsilon^{WT}(h = \alpha - d)$ . These observations seriously question the validity of most of the experimental and numerical BC estimates of the  $\tau_\epsilon^{BC}(q)$  and  $f_\epsilon^{BC}(\alpha)$  spectra reported so far in the literature. In Fig. 3(d) is shown for comparison some average  $f_\epsilon^{BC}(\alpha)$  spectrum obtained by Meneveau and Sreenivasan [3] for 1D surrogate dissipation experimental data ( $d = 1$ ). We notice that these experimental data were claimed to be well fitted by the conservative p-model with  $p = 0.3$  ( $1 - p = 0.7$ ), i.e. a value not so far from the value  $p = p_1 / (p_1 + p_2) = 0.32$

derived from our 3D WTMM method.

To conclude, let us point out that previous application of the 1D WTMM method to 1D surrogate dissipation data has already revealed the fact that the cancellation exponent might be different from zero [18]. What the 3D WTMM results reported in this letter show, is that this surprising result is not some artefact resulting from the analysis of 1D cuts (the dissipation could well be non conserved along these cuts), but that the multifractal spatial structure of the 3D dissipation field is likely to be well described by a multiplicative cascade process that is definitely non conservative. As shown in Fig. 3(d), the  $f_\epsilon^{WT}(\alpha)$  data seem to be even better fitted by a parabola, as predicted for non-conservative log-normal cascade processes. There is no doubt that such a result together with future WTMM multifractal analysis of velocity, dissipation and enstrophy fields data will provide new insight into the multifractal description of intermittency in fully-developed turbulence.

We are very grateful to M. Meneguzzi for allowing us to have access to his DNS data.

- 
- [1] T. C. Halsey *et al.*, Phys. Rev. A **33**, 1141 (1986).
  - [2] B. B. Mandelbrot, J. Fluid Mech. **62**, 331 (1974).
  - [3] C. Meneveau and K. R. Sreenivasan, J. Fluid Mech. **224**, 429 (1991).
  - [4] U. Frisch, *Turbulence* (Cambridge Univ. Press, Cambridge, 1995).
  - [5] P. Grassberger and I. Procaccia, Physica D **9**, 189 (1983).
  - [6] G. Parisi and U. Frisch, in *Turbulence and Predictability in Geophysical Fluid Dynamics and Climate Dynamics, Proc. of Int. School*, edited by M. Ghil, R. Benzi, and G. Parisi (North-Holland, Amsterdam, 1985), p. 84.
  - [7] J. F. Muzy, E. Bacry, and A. Arneodo, Int. J. of Bifurcation and Chaos **4**, 245 (1994); A. Arneodo, E. Bacry, and J. F. Muzy, Physica A **213**, 232 (1995).
  - [8] A. Arneodo *et al.*, *Ondelettes, Multifractales et Turbulences : de l'ADN aux croissances cristallines* (Diderot Editeur, Art et Sciences, Paris, 1995).
  - [9] *The Science of Disasters : climate disruptions, heart attacks and market crashes*, edited by A. Bunde, J. Kropp, and H. Schellnhuber (Springer Verlag, Berlin, 2002).
  - [10] A. Arneodo, N. Decoster, and S. G. Roux, Eur. Phys. J. B **15**, 567 (2000); N. Decoster, S. G. Roux, and A. Arneodo, Eur. Phys. J. B **15**, 739 (2000).
  - [11] A. Arneodo, N. Decoster, and S. G. Roux, Phys. Rev. Lett. **83**, 1255 (1999); S. G. Roux, A. Arneodo, and N. Decoster, Eur. Phys. J. B **15**, 765 (2000).
  - [12] P. Kestener *et al.*, Image Anal. Stereol. **20**, 169 (2001).
  - [13] S. Mallat and W. L. Hwang, IEEE Trans. on Information Theory **38**, 617 (1992).
  - [14] D. Schertzer, and S. Lovejoy, J. Geophys. Res. **92**, 9693 (1987).
  - [15] (a) S. Chen *et al.*, Phys. Fluids A **5**, 458 (1992); (b) L. P. Wang *et al.*, J. Fluid Mech. **309**, 113 (1996); (c) I. Hosokawa, S. *et al.*, Phys. Rev. Lett. **77**, 4548 (1996); (d) A. Bershadskii *et al.*, Eur. Phys. J. B **18**, 95 (2000).

- [16] A. Vincent and M. Meneguzzi, *J. Fluid Mech.* **225**, 1 (1995).
- [17] E. Ott *et al.*, *Phys. Rev. Lett.* **69**, 2654 (1992).
- [18] S. G. Roux, Ph.D. thesis, University of Aix-Marseille II, 1996, unpublished.